2007 IEEE International Conference on
Robotics and Automation
Roma, Italy, 10-14 April 2007

Iterative Learning of Specified Motions in Task-Space for Redundant Multi-Joint Hand-Arm Robots

Suguru Arimoto, Masahiro Sekimoto, and Sadao Kawamura

***Abstract*— This paper proposes an iterative learning control (ILC) scheme for a class of redundant robot arms to acquire the desired control input signals that produce an endpoint trajectory specified in task space. The learning update law of control input signals is constructed only in task space by modifying the previous control input through adding linearly an endpoint velocity trajectory error. Although the dimension of the task space is strictly less than the DOF (Degrees-of-freedom) of the robot arm, the proposed method need neither consider any inverse kinematics problem nor introduce any cost function to be optimized and to determine the inverse kinematics (or dynamics) uniquely. Convergence of trajectory trackings to the specified one is shown by numerical simulations in both cases 1) free-endpoint motion and 2) constraint-endpoint motion with specified contact force. A theoretical proof of convergences in the case of free-endpoint motion is given on the basis of an approximated dynamics linearized around a desired solution in joint state space.**

I. INTRODUCTION

When infants of 3 to 5 months old start to learn reaching for an object and grasping, they gaze at the object but do not see any motion of the arm as pointed out in many observations obtained in experimental and developmental psychology [1], [2]. Even in case of well matured adults, the first trial in learning to reach a target point and write a circle on a black board is primarily a problem of control of the arms through haptic and proprioceptive information. Later, in repetition of the exercises, they rely increasingly on vision to refine trajectories in the task space and focus to adjust the arm endpoint (maybe, a white chalk) to their envisioned target trajectory. During such fine-tuning processes, they do not watch movements of arm joints such as wrist, elbow, and shoulder joints.

Accurate trajectory tracking can be achieved theoretically in case of robot arms by using feedforward model-based control laws called the computed torque method. However, this methodology may produce unsatisfactory results when parametric uncertainties in arm dynamics are present to some extent and/or unmodeled dynamics of actuators and payloads are supposed to exist. To cope with this parameter-uncertainty problem, an appealing approach of trajectory tracking for robotic systems with uncertain or unknown parameters was proposed in 1984 [3], later called the iterative learning control (ILC) and widely investigated not only in trajectory tracking of robotic systems [4] but also in control of repetitive tasks for mechatronics systems. However, in most papers of the literature on ILC except the paper by De Luca and Mataloni [5], only a family of objective dynamics whose number of DOFs is equal to the dimension of physical variables of task space, that is, non-redundant dynamics, have been treated as far as nonlinear robot dynamics is concerned, though it has been believed at least among roboticists that surplus DOFs in robotic systems may offer advantages in executing dexterous tasks. The reason is that redundancy in DOFs of objective dynamics, on the other hand, may incur illposedness of inverse kinematics and make the control problems more sophisticated. It was very recent that even in case of redundant arms a task space PD feedback for multi-joint reaching produces satisfactory skilled motions without calculating the pseudo inverse of a Jacobian matrix or introduce any cost function to determine the inverse kinematics uniquely [6]–[8]. In the problem of Point-to-Point (PTP) reaching, there is no need of planning a trajectory in the task space in advance. On the other side, there is a vast literature of research works on PTP reaching for redundant robots which are based upon planning an optimized trajectory in joint space by introducing an artificial performance index such as "manipulability," "kinetic energy," and "quadratic functions of acceleration, jerk, or torque," etc. Once the optimal trajectory in some sense is determined in joint space, the problem is of application of the computed torque to tracking control in joint level. Thus, very recently, Nakanishi *et al.* [9] showed interesting results on comparative and quantitative studies on performances of task space trajectory tracking among such optimization techniques for redundant robots.

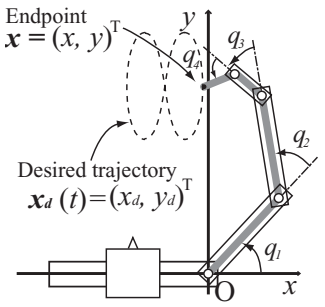

Fig. 1. Planar movement by a robot arm with four DOFs.

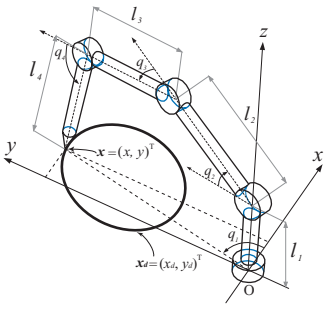

Fig. 2. A hand writing robot model with four DOFs

This work was in part supported by the Grant-in-Aid for Exploratory Research of the JSPS (Subject No. 16656085), and MEXT. HAITEKU (2004–2008).

S. Arimoto is with (1) the Department of Robotics, Ritsumeikan University, 1-1-1 Nojihigashi, Kusatsu, Shiga 525-8577, Japan, and (2) the BMC Research Center, RIKEN, 2271-130 Anagahora, Shimoshidami, Moriyama, Nagoya, Aichi 463-0003, Japan arimoto@se.ritsumei.ac.jp

M. Sekimoto and S. Kawamura are with the Department of Robotics, Ritsumeikan University, 1-1-1 Nojihigashi, Kusatsu, Shiga 525-8577, Japan {rr006993, kawamura}@se.ritsumei.ac.jp

This paper extends the conventional ILC scheme for joint space motion-trajectory tracking to that for task space motion-trajectory tracking in the case that the number of physical variables (or dimension) necessary and sufficient for description of a given task in task space is less than the total DOFs of an objective robot arm. Differently from De Luca *et al.*'s approach [5] [10] based upon frequency-domain, our proposed learning update law is quite of a simple form and constructed in time-domain in such a way that the next control signal is composed in task space of a linear sum of the present control signal and the task space velocity-error signal with a constant coefficient. When this control input is applied for making the next trial, it is exerted at arm joints in a feedforward manner through the transpose of the Jacobian matrix of physical variables in task space with respect to arm joint variables. Verification of the effectiveness of the proposed method is shown in computer simulations in both cases 1) of using a 4 DOF planar robot for the task of writing a Lissajous or triangle figure (Fig.1) and 2) of using a 4 DOF hand-writing robot whose endpoint is constrained on a xy-plane and requested to write a circle with a specified pressing force (Fig.2). A theoretical verification of convergence of the ILC scheme is also presented by using a time-varying dynamics linearized around an ideal joint motion that achieves the desired task.

II. FREE-ENDPOINT MOTION: A HUMAN-LIKE ROBOT ARM WITH REDUNDANT DOFS

Lagrange's equation of motion of a multijoint system whose motion is confined to a horizontal plane (Fig.1) [4] is described by:

$$H(\boldsymbol{q})\ddot{\boldsymbol{q}} + \left\{\frac{1}{2}\dot{H}(\boldsymbol{q}) + S(\boldsymbol{q}, \dot{\boldsymbol{q}})\right\}\dot{\boldsymbol{q}} = \boldsymbol{u} \tag{1}$$

where $\boldsymbol{q} = (q_1, q_2, q_3, q_4)^{\mathrm{T}}$ denotes the vector of joint angles, $H(\boldsymbol{q})$ is the inertia matrix, $S(\boldsymbol{q}, \dot{\boldsymbol{q}})\dot{\boldsymbol{q}}$ is the gyroscopic force term including centrifugal and Coriolis forces, $\boldsymbol{u}$ is the control input torque at joints defined as:

$$\boldsymbol{u} = -C\dot{q} - J(q)^{\mathrm{T}}\left\{k\Delta\boldsymbol{x}(t) + \zeta_1\sqrt{k}\Delta\dot{x}(t) - \boldsymbol{v}_n(t)\right\} \tag{2}$$

where C denotes a positive definite and diagonal damping coefficient matrix (i.e., $C = \mathrm{diag}(c_1, \ldots, c_4)$ where $c_i > 0$), $J(\boldsymbol{q})$ is the Jacobian matrix of task coordinates $\boldsymbol{x}$ in joint coordinates q, $\Delta\boldsymbol{x}(t) = \boldsymbol{x}(t) - \boldsymbol{x}_d(t)$, and k and ζ_1 are positive constant gain parameters. $\boldsymbol{v}_n(t)$ stands for a feedforward learning update law determined by:

$$\boldsymbol{v}_n(t) = \begin{cases} \boldsymbol{0} & (n = 1) \\ \boldsymbol{v}_{n-1}(t) - \Phi\Delta\dot{\boldsymbol{x}}_{n-1}(t) & (n > 1) \end{cases} \tag{3}$$

where n denotes the trial number, $\Delta\boldsymbol{x}_n(t) = \boldsymbol{x}_n(t) - \boldsymbol{x}_d(t)$, and Φ is a positive constant parameter for ILC. Then, by substituting eq.(2) into eq.(1), we obtain the closed-loop dynamics at the n-th trial as follows:

$$H(\boldsymbol{q}_n)\ddot{\boldsymbol{q}}_n + \left\{\frac{1}{2}\dot{H}(\boldsymbol{q}_n) + S(\boldsymbol{q}_n, \dot{\boldsymbol{q}}_n) + C\right\}\dot{\boldsymbol{q}}_n + J^{\mathrm{T}}(\boldsymbol{q}_n)\left\{k\Delta\boldsymbol{x}_n + \zeta_1\sqrt{k}\Delta\dot{\boldsymbol{x}}_n\right\} = J^{\mathrm{T}}(\boldsymbol{q}_n)\boldsymbol{v}_n \tag{4}$$

In order to gain a physical insight into the problem of convergence of $\Delta\dot{\boldsymbol{x}}_n$ to zero with the increase of n, it is convenient to transpose $\dot{\boldsymbol{q}}_n$ into

$$\dot{\boldsymbol{q}}_n = \left(J_n^+(\boldsymbol{q}_n),\, P_n\right)\begin{pmatrix} \dot{\boldsymbol{x}}_n \\ \dot{\boldsymbol{y}}_n \end{pmatrix} \tag{5}$$

where

$$J_n^+ = J_n^{\mathrm{T}}(J_n J_n^{\mathrm{T}})^{-1}, \tag{6}$$

and P_n is a 4×2-matrix orthogonal to $J_n^+(\boldsymbol{q}_n)$, i.e., $P_n^{\mathrm{T}}J_n^+ = 0_{4\times 4}$, with a property that $P_n = (\boldsymbol{p}_1, \boldsymbol{p}_2)$, $\boldsymbol{p}_i$ denotes a 4×1 column vector with $\|\boldsymbol{p}_i\| = 1$ and $\boldsymbol{p}_1^{\mathrm{T}}\boldsymbol{p}_2 = 0$. Then, it is easy to see that if we define

$$Q_n = \left(J_n^+, P_n\right), \quad Q_n^{-1} = \begin{pmatrix} J_n \\ P_n^{\mathrm{T}} \end{pmatrix}, \tag{7}$$

$$Q_n^{\mathrm{T}}H(\boldsymbol{q}_n)Q_n = H_n, \tag{8}$$

$$S_n = Q_n^{\mathrm{T}}SQ_n - \frac{1}{2}\dot{Q}_n^{\mathrm{T}}HQ_n + \frac{1}{2}Q_n^{\mathrm{T}}H\dot{Q}_n \tag{9}$$

then, by substituting eq.(5) into eq.(4) and multiplying the resultant equation by the transpose of Q_n from the left-hand, we have

$$H_n\begin{pmatrix} \ddot{\boldsymbol{x}}_n \\ \ddot{\boldsymbol{y}}_n \end{pmatrix} + \left\{\frac{1}{2}\dot{H}_n + S_n + Q_n^{\mathrm{T}}CQ_n\right\}\begin{pmatrix} \dot{\boldsymbol{x}}_n \\ \dot{\boldsymbol{y}}_n \end{pmatrix} + \zeta_1\sqrt{k}\begin{pmatrix} \Delta\dot{\boldsymbol{x}}_n \\ \boldsymbol{0} \end{pmatrix} + k\begin{pmatrix} \Delta\boldsymbol{x}_n \\ \boldsymbol{0} \end{pmatrix} = \begin{pmatrix} \boldsymbol{v}_n \\ \boldsymbol{0} \end{pmatrix} \tag{10}$$

In this paper, to gain a physical insight into the problem of convergence of trajectories $\Delta\dot{\boldsymbol{x}}_n(t)$, we assume that there exists an ideal control signal $\boldsymbol{v}_d(t)$ so that it satisfies

$$H_d\begin{pmatrix} \ddot{\boldsymbol{x}}_d \\ \ddot{\boldsymbol{y}}_d \end{pmatrix} + \left\{\frac{1}{2}\dot{H}_d + S_d + Q_d^{\mathrm{T}}CQ_d\right\}\begin{pmatrix} \dot{\boldsymbol{x}}_d \\ \dot{\boldsymbol{y}}_d \end{pmatrix} = \begin{pmatrix} \boldsymbol{v}_d \\ \boldsymbol{0} \end{pmatrix} \tag{11}$$

where $Q_d = (J_d^+(\boldsymbol{q}_d),\, P(\boldsymbol{q}_d))$, $H_d = Q_d^{\mathrm{T}}H(\boldsymbol{q}_d)Q_d$, $S_d = Q_d^{\mathrm{T}}S(\boldsymbol{q}_d,\, \dot{\boldsymbol{q}}_d)Q_d - \frac{1}{2}\dot{Q}_d^{\mathrm{T}}HQ_d + \frac{1}{2}Q_d^{\mathrm{T}}H\dot{Q}_d$. For convenience, we define

$$B_d = \frac{1}{2}\dot{H}_d + S_d + Q_d^{\mathrm{T}}CQ_d \tag{12}$$

Then, it follows from eq.(11) that

$$H_{22}\ddot{\boldsymbol{y}}_d + B_{22}\dot{\boldsymbol{y}}_d = -H_{12}^{\mathrm{T}}\ddot{\boldsymbol{x}}_d - B_{21}\dot{\boldsymbol{x}}_d \tag{13}$$

where

$$H_d = \begin{pmatrix} H_{11} & H_{12} \\ H_{12}^{\mathrm{T}} & H_{22} \end{pmatrix}, \quad B_d = \begin{pmatrix} B_{11} & B_{12} \\ B_{21} & B_{22} \end{pmatrix} \tag{14}$$

Equation (13) means that if $\dot{\boldsymbol{x}}_d$, $\ddot{\boldsymbol{x}}_d$, and $\boldsymbol{q}_d$ are given then $\dot{\boldsymbol{y}}_d$ is determined uniquely from solving the differential equation of eq.(13) under the initial condition $\dot{\boldsymbol{y}}_d(0) = \boldsymbol{0}$. Furthermore, we discuss the problem of convergence of trajectory trackings based upon a linearized dynamics of the

TABLE I

PHYSICAL PARAMETERS OF THE 4-DOF ROBOT ARM

Link number	i	1	2	3	4
Length [m]	l_i	0.2800	0.2800	0.09500	0.09000
Center of mass [m]	l_{gi}	0.1400	0.1400	0.04750	0.04500
Cylinder radius [m]	r_i	0.04000	0.03500	N/A	0.009500
Cuboid height [m]	h_i	N/A	N/A	0.08500	N/A
Cuboid depth [m]	d_i	N/A	N/A	0.03000	N/A
Mass [kg]	m_i	1.407	1.078	0.2423	0.02552
Inertia moment [kgm^2]	I_{giz}	9.758×10^{-3}	7.370×10^{-3}	2.004×10^{-4}	1.780×10^{-5}

TABLE II

INITIAL VALUES AND GAIN SETTINGS IN THE CASE OF THE 4-DOF PLANAR ROBOT ARM

Terminal time	T	2.0 [s]
Initial posture	$q_1(0)$	21.02 [deg]
	$q_2(0)$	75.47 [deg]
	$q_3(0)$	44.20 [deg]
	$q_4(0)$	64.87 [deg]

Gains	k	10 [N/m]
	ζ_0	0.5 [-]
	ζ_1	2.5 [-]
	Φ	7.0 [-]
	c_1	0.862 [Nms]
	c_2	0.569 [Nms]
	c_3	0.129 [Nms]
	c_4	0.0356 [Nms]

TABLE III

NUMERICAL VALUES OF INERTIA MATRIX $H(q(t))$ AT $t = 0$ IN THE CASE OF THE 4-DOF PLANAR ROBOT ARM (UNIT: kgm^2)

$$H(q(0)) = \begin{bmatrix} 2.260 \times 10^{-1} & 6.962 \times 10^{-2} & 1.580 \times 10^{-3} & -3.097 \times 10^{-4} \\ 6.962 \times 10^{-2} & 5.601 \times 10^{-2} & 3.831 \times 10^{-3} & 1.080 \times 10^{-5} \\ 1.580 \times 10^{-3} & 3.831 \times 10^{-3} & 1.139 \times 10^{-3} & 1.158 \times 10^{-4} \\ -3.097 \times 10^{-4} & 1.080 \times 10^{-5} & 1.158 \times 10^{-4} & 6.947 \times 10^{-5} \end{bmatrix}$$

robot around the ideal joint velocity and position vector $\dot{\boldsymbol{q}}_d(t)$ and $\boldsymbol{q}_d(t)$, that is described as

$$H_d(t)\begin{pmatrix} \ddot{\boldsymbol{x}}_n \\ \ddot{\boldsymbol{y}}_n \end{pmatrix} + \left\{ \frac{1}{2}\dot{H}_d(t) + S_d(t) + Q_d^{\mathrm{T}}(t) C Q_d(t) \right\} \begin{pmatrix} \dot{\boldsymbol{x}}_n \\ \dot{\boldsymbol{y}}_n \end{pmatrix} + \zeta_1 \sqrt{k} \begin{pmatrix} \Delta\dot{\boldsymbol{x}}_n \\ \boldsymbol{0} \end{pmatrix} + k \begin{pmatrix} \Delta\boldsymbol{x}_n \\ \boldsymbol{0} \end{pmatrix} = \begin{pmatrix} \boldsymbol{v}_n \\ \boldsymbol{0} \end{pmatrix} \quad (15)$$

Then, subtraction of eq.(11) from eq.(15) yields

$$H_d(t)\begin{pmatrix} \Delta\ddot{\boldsymbol{x}}_n \\ \Delta\ddot{\boldsymbol{y}}_n \end{pmatrix} + \left\{ \frac{1}{2}\dot{H}_d + S_d + Q_d^{\mathrm{T}} C Q_d \right\} \begin{pmatrix} \Delta\dot{\boldsymbol{x}}_n \\ \Delta\dot{\boldsymbol{y}}_n \end{pmatrix} + \zeta_1 \sqrt{k} \begin{pmatrix} \Delta\dot{\boldsymbol{x}}_n \\ \boldsymbol{0} \end{pmatrix} + k \begin{pmatrix} \Delta\boldsymbol{x}_n \\ \boldsymbol{0} \end{pmatrix} = \begin{pmatrix} \Delta\boldsymbol{v}_n \\ \boldsymbol{0} \end{pmatrix} \quad (16)$$

where $\Delta\boldsymbol{v}_n = \boldsymbol{v}_n - \boldsymbol{v}_d$. Then, taking an inner product between this equation and vector $(\Delta\dot{\boldsymbol{x}}_n^{\mathrm{T}}, \Delta\dot{\boldsymbol{y}}_n^{\mathrm{T}})^{\mathrm{T}}$ yields

$$\int_0^t \Delta\dot{\boldsymbol{x}}_n^{\mathrm{T}}(\tau)\Delta\boldsymbol{v}_n(\tau)\mathrm{d}\tau = E_{dn}(t) - E_{dn}(0) + \int_0^t \left\{ \zeta_1\sqrt{k}\|\Delta\dot{\boldsymbol{x}}_n\|^2 + (\Delta\dot{\boldsymbol{x}}_n^{\mathrm{T}}, \Delta\dot{\boldsymbol{y}}_n^{\mathrm{T}})\, Q_d^{\mathrm{T}} C Q_d\, (\Delta\dot{\boldsymbol{x}}_n^{\mathrm{T}}, \Delta\dot{\boldsymbol{y}}_n^{\mathrm{T}})^{\mathrm{T}} \right\} \mathrm{d}\tau \quad (17)$$

where

$$E_{dn} = \frac{1}{2}(\Delta\dot{\boldsymbol{x}}_n^{\mathrm{T}}, \Delta\dot{\boldsymbol{y}}_n^{\mathrm{T}}) H_d (\Delta\dot{\boldsymbol{x}}_n^{\mathrm{T}}, \Delta\dot{\boldsymbol{y}}_n^{\mathrm{T}})^{\mathrm{T}} + \frac{1}{2}k\|\Delta\boldsymbol{x}_n\|^2 \quad (18)$$

Since $E_{dn} \geq 0$, and $Q_d^{\mathrm{T}} C Q_d$ is positive definite, eq.(17) shows the passivity of eq.(16) concerning the input-output pair $\left\{ (\Delta\boldsymbol{v}_n^{\mathrm{T}}, \boldsymbol{0}^{\mathrm{T}})^{\mathrm{T}},\ (\Delta\dot{\boldsymbol{x}}_n^{\mathrm{T}}, \Delta\dot{\boldsymbol{y}}_n^{\mathrm{T}})^{\mathrm{T}} \right\}$.

Convergence of trajectory trackings in task space as $n \to \infty$ can be proved by using the passivity relation of eq.(17). The details will be given in Appendix A.

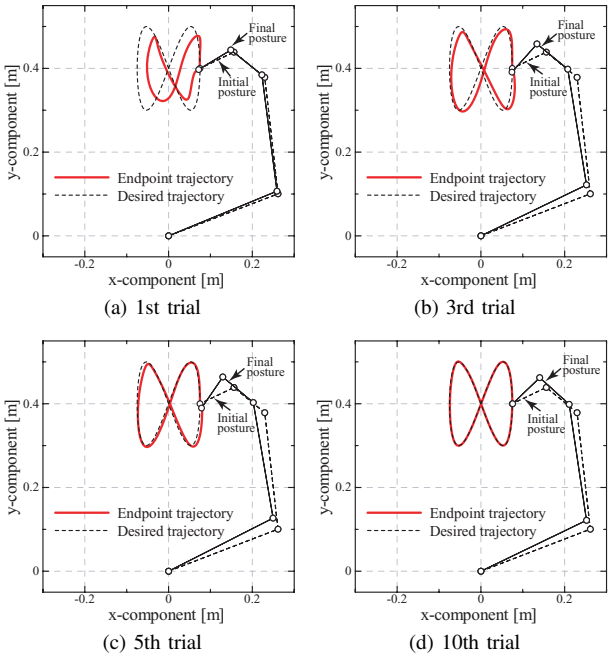

(a) 1st trial (b) 3rd trial (c) 5th trial (d) 10th trial

Fig. 3. Endpoint trajectories and the initial and final postures of the arm

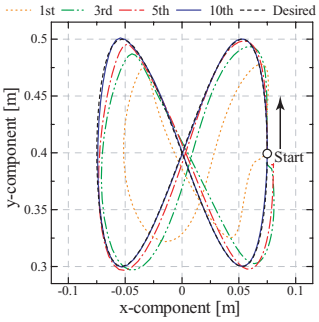

Fig. 4. Endpoint trajectories

III. NUMERICAL SIMULATIONS

In order to verify the effectiveness of the proposed ILC scheme shown in eq.(2), we conducted some numerical simulations. Physical parameters of the robot arm are set as shown in TABLE I (these are just similar to those of an average adult arm), and the robot is requested to write a specified figure — Lissajous or triangle —.

First, in order to draw a Lissajous figure at the endpoint of the robot arm, the following desired trajectory is given:

$$\boldsymbol{x}_d(t) = \begin{bmatrix} 0.00 \\ 0.40 \end{bmatrix} + \begin{bmatrix} 0.075\cos\omega(t) \\ 0.10\sin 2\omega(t) \end{bmatrix} \ [\mathrm{m}] \quad (19)$$

where

$$\omega(t) = 2.0\pi \left\{ -15\left(\frac{t}{T}\right)^4 + 6\left(\frac{t}{T}\right)^5 + 10\left(\frac{t}{T}\right)^3 \right\} \quad (20)$$

where T denotes the terminal time of the desired trajectory. We remark that $\boldsymbol{x}_d(t)$ is given to be twice continuously differentiable and both $\dot{\boldsymbol{x}}_d(t)$ and $\ddot{\boldsymbol{x}}_d(t)$ must vanish at initial time $t = 0$ and terminal time $t = T$. Initial posture and gain parameters are set as shown in TABLE II the same through all the trials, that is, the posture of the whole robot

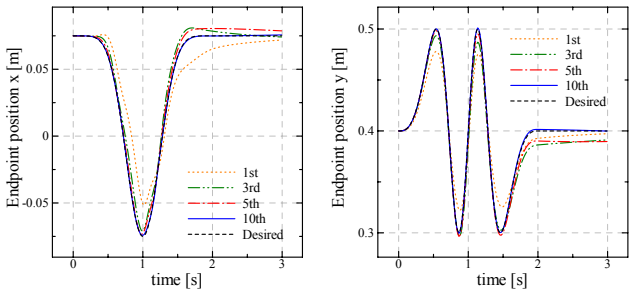

(a) x (b) y

Fig. 5. Transient responses of endpoint positions

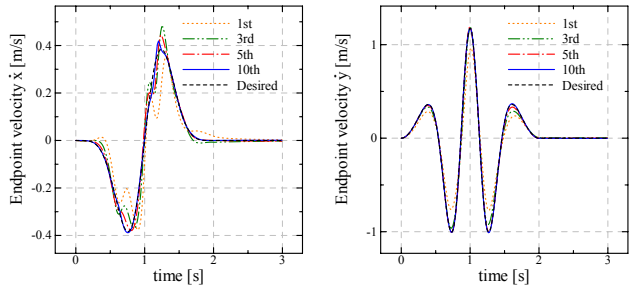

(a) $\dot{x}$ (b) $\dot{y}$

Fig. 6. Transient responses of endpoint velocity

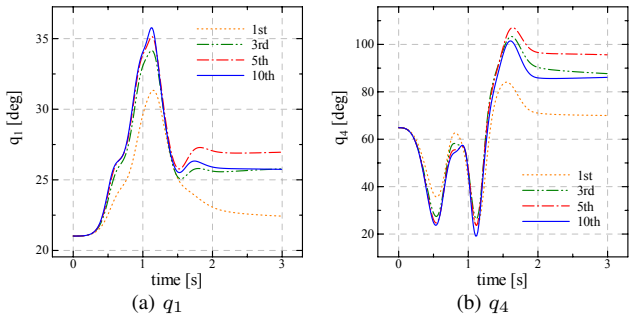

(a) q_1 (b) q_4

Fig. 7. Transient responses of arm joints

is initialized by the same values at every trial. Furthermore, the endpoint at the initial time should be set so as to coincide with the desired trajectory at $t = 0$ ($\boldsymbol{x}(0) = \boldsymbol{x}_d(0)$). As discussed detailedly in our previous paper [6] as for synergistic choice among a group of joint dampings in the control signal of eq.(2), damping matrix C may be chosen as being of order of the square root of initial inertia matrix $H(\boldsymbol{q}(0))$. In this simulation, the damping factors are chosen as follows:

$$c_i = \zeta_0 \sqrt{k} \sqrt{\sum_{j=1}^{4} |H_{ij}(\boldsymbol{q}(0))|} \qquad (i = 1, \ldots, 4) \qquad (21)$$

where $H = (H_{ij})$. In the case of the initial posture in TABLE II, initial values of inertia matrix $H(\boldsymbol{q}(0))$ are evaluated as in TABLE III. Simulation results in this case are presented in Figs.3-7. Figure 3 shows endpoint trajectories and initial and final postures at each trial, Fig.4 shows endpoint trajectories, Figs.5-7 show time responses of endpoint position, velocity, and joint angles respectively. As seen in Figs.3-7, at the first trial (before learning) the endpoint trajectory is far from the desired trajectory but at the 10th trial (after having learned)

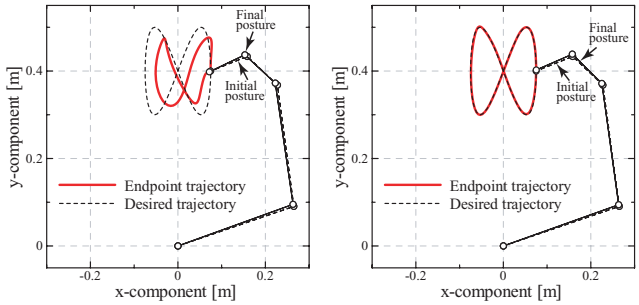

(a) 1st trial (b) 10th trial

Fig. 8. Endpoint trajectories and the initial and final postures of the arm when a different initial posture ($\boldsymbol{q}(0) = (18.84,\ 78.83,\ 38.88,\ 65.13)^{\mathrm{T}}$ [deg]) is set

TABLE IV

TARGET POSITIONS FOR TRIANGLE FIGURE

$\boldsymbol{x}_{v(0)}$	$(0.10,\ 0.40)^{\mathrm{T}}$ [m]
$\boldsymbol{x}_{v(1)}$	$(0.00,\ 0.573)^{\mathrm{T}}$ [m]
$\boldsymbol{x}_{v(2)}$	$(-0.10,\ 0.40)^{\mathrm{T}}$ [m]
$\boldsymbol{x}_{v(3)}$	$(0.10,\ 0.40)^{\mathrm{T}}$ [m]

TABLE V

INITIAL VALUES AND GAIN SETTINGS FOR TRIANGLE FIGURE TRAJECTORY

Terminal time	T	1.0 [s]
Initial posture	$q_1(0)$	19.35 [deg]
	$q_2(0)$	73.50 [deg]
	$q_3(0)$	43.47 [deg]
	$q_4(0)$	68.67 [deg]

Gains	k	10 [N/m]
	ζ_0	0.5 [-]
	ζ_1	2.5 [-]
	Φ	7.0 [-]
	c_1	0.873 [Nms]
	c_2	0.574 [Nms]
	c_3	0.131 [Nms]
	c_4	0.0361 [Nms]

it can accurately follow the desired trajectory, and the pose of the arm during its movement does not become unnatural through all the trials. As pointed out by Seraji [11] as for robot arms with redundant DOFs, self-motion may arise during or even after the end of trajectory tracking due to joint DOF redundancy. Therefore, we run the simulations for one more second after the terminal time of trajectory tracking by setting the same desired position, which is fixed as $\boldsymbol{x}_d(t) = \boldsymbol{x}_d(T)$, $\dot{\boldsymbol{x}}_d(t) = \boldsymbol{0}$ for $T < t \leq (T + 1.0)$. As seen in Fig.7, after repetition of trials (at the 10th trial), the joints does not move after the end of the trajectory tracking (after 2[s]), and self-motion does not arise. According to the results in Fig.7, the joints move after 2[s] at the 1st and 3rd trials. This happened when the endpoint is far from the desired position, because the force ($-k\Delta\boldsymbol{x}$) leading the endpoint to the target still remains even after 2 [s]. Therefore, this phenomenon is different from self-motion. In order to demonstrate versatility of the proposed ILC scheme, we conducted another simulations by using different initial arm postures. Figure 8 shows one of simulation results when one initial arm pose different from the settings of TABLE II is chosen but the gain settings are the same as in the previous simulation. As seen from Fig.8, the proposed ILC scheme is almost equally effective among choices of different initial poses to some extent.

Next, in order to let the robot arm to write a triangle on the xy-plane, we define

$$\boldsymbol{x}_d(t) = \begin{cases} \boldsymbol{x}_{v(n)} + \{\boldsymbol{x}_{v(n+1)} - \boldsymbol{x}_{v(n)}\}\ \omega(t - T_{(n)}) \\ \qquad\qquad (T_{(n)} \le t < T_{(n)} + T) \\ \boldsymbol{x}_{v(n+1)} \qquad\qquad (T_{(n)} + T \le t < T_{(n+1)}) \end{cases} \quad (22)$$
$$(n = 0,\ 1,\ 2)$$

where $T_{(n)} = n(T + 0.5)$ and vertex positions of the triangle are set as shown in TABLE IV. Figure 9 shows simulation results in the case that the initial posture and gains are chosen as in TABLE V. The gain settings (k, ζ_0, ζ_1, and Φ) are entirely the same as those in the previous simulations. Nevertheless at the 10th trial the endpoint accomplishes the desired trajectory without incurring self-motion. Even in the cases that other figures or different time intervals are given, exact trajectory tracking could be realized after a sufficient repetition of trials.

In the conventional ILC scheme for non-redundant DOF robots, the learning update law which consists of a linear sum of the task space position-error signal together with the velocity-error signal (called PI-type learning) has been also proposed [4]. Therefore, we conducted simulations by using the following update law:

$$\boldsymbol{v}_n(t) = \boldsymbol{v}_{n-1}(t) - \{\Phi \Delta \dot{\boldsymbol{x}}_{n-1}(t) + \Psi \Delta \boldsymbol{x}_{n-1}(t)\} \quad (23)$$

where Ψ denotes a positive constant parameter. Figure 10 shows simulation results in the case that the desired trajectory of eq.(22) is chosen and initial values and gains in TABLE V and $\Psi = 4.0$ are set. As seen in Fig.10, the endpoint trajectory approaches closely to the desired trajectory after a few trials in comparison with Fig.9. Though the simulation results in Fig.10 do not directly indicate superiority of the learning update law of eq.(23) to eq.(3), it must work efficiently in the case that effects of Coulomb friction inherent to robots are large (e.g. industrial robots).

IV. ENDPOINT-CONSTRAINT MOTION: HAND-WRITING ROBOT

Next, as an example of trajectory tracking in task space under holonomic constraints, we consider a hand-writing robot with four joints shown in Fig.2. In this case, dynamics of the robot can be described by the following Lagrange equation of motion with a holonomic constraint $\phi(\boldsymbol{q}) = 0$:

$$H(\boldsymbol{q})\ddot{\boldsymbol{q}} + \left\{\frac{1}{2}\dot{H}(\boldsymbol{q}) + S(\boldsymbol{q}, \dot{\boldsymbol{q}})\right\}\dot{\boldsymbol{q}} + g(\boldsymbol{q}) - \frac{\partial \phi}{\partial \boldsymbol{q}}\lambda = \boldsymbol{u} \quad (24)$$

where $g(\boldsymbol{q})$ denotes the gravity term and λ is a Lagrange multiplier corresponding to the constraint $\phi = 0$. In this case, the endpoint (the pen nib) should be kept on the xy-plane during hand-writing motion. This is expressed as a constraint equation as follows:

$$\phi = l_1 + l_2 \sin q_2 + l_3 \sin(q_2 + q_3) + l_4 \sin(q_2 + q_3 + q_4) = 0 \quad (25)$$

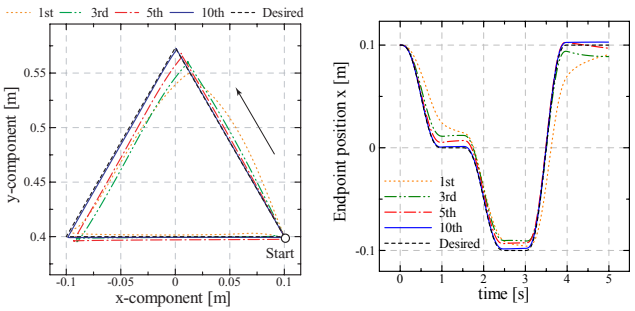

(a) Endpoint trajectories (b) x

Fig. 9. Transient responses when a desired trajectory of triangle figure is given

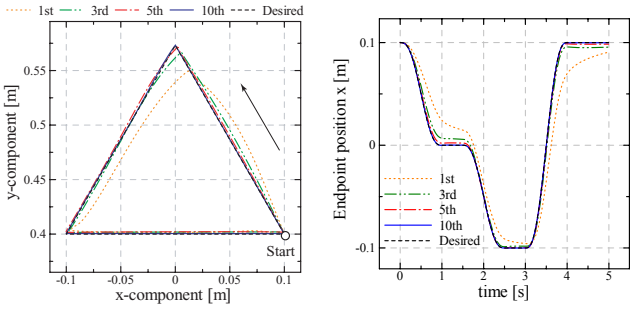

(a) Endpoint trajectories (b) x

Fig. 10. Transient responses when a desired trajectory of triangle figure is given and the learning update law of PI-type is used

Once the constraint is defined by eq.(25), the corresponding Lagrange multiplier λ together with gradient vector $(\partial\phi/\partial\boldsymbol{q})$ plays a role of the the contact force orthogonal to the xy-plane (in detail, see [8]). Physical parameters of the robot are shown in TABLE VI.

The objective task is to accomplish a desired trajectory tracking while maintaining a specified contact force at the endpoint. Based on the previous works [8], [12], we consider the following control signal:

$$\boldsymbol{u} = -C\dot{\boldsymbol{q}} - J^{\mathrm{T}}(\boldsymbol{q})\left\{k\Delta\boldsymbol{x}(t) + \zeta_1\sqrt{k}\Delta\dot{\boldsymbol{x}}(t) - \boldsymbol{v}_k(t)\right\} - \frac{\partial\phi}{\partial\boldsymbol{q}}\{\lambda_d - \sigma_n(t)\} + g(\boldsymbol{q}) \quad (26)$$

where λ_d denotes a desired contact force (positive constant), $\boldsymbol{v}_n(t)$ is equivalent to the update law shown in eq.(3), and

$$\sigma_n(t) = \sigma_{n-1}(t) + \Lambda\Delta\lambda_{n-1}(t) \quad (27)$$

where $\Delta\lambda_{n-1}(t) = \lambda_{n-1}(t) - \lambda_d$. Equation (27) means the learning update law to accomplish the desired contact force.

In numerical simulation, drawing a circle on a sheet (xy-plane) is imposed by setting the following desired trajectory:

$$\boldsymbol{x}_d(t) = \begin{bmatrix} 0.00 \\ 0.23 \end{bmatrix} + 0.05 \begin{bmatrix} \sin\omega(t) \\ -\cos\omega(t) \end{bmatrix}\ [\mathrm{m}] \quad (28)$$

where

$$\omega(t) = 2.0\pi\left\{-2\left(\frac{t}{T}\right)^3 + 3\left(\frac{t}{T}\right)^2\right\} \quad (29)$$

TABLE VI

LINK PARAMETERS OF THE HAND-WRITING ROBOT

Link number	i	1	2	3	4
Length [m]	l_i	0.096	0.100	0.100	0.167
Mass [kg]	m_i	0.111	0.102	0.102	0.052

TABLE VII

INITIAL VALUES AND GAIN SETTINGS IN THE CASE OF DRAWINGS BY THE HAND-WRITING ROBOT

Terminal time	T	1.0 [s]
Initial posture	$q_1(0)$	90.00 [deg]
	$q_2(0)$	55.71 [deg]
	$q_3(0)$	-63.43 [deg]
	$q_4(0)$	-73.82 [deg]
Desired force	λ_d	1.0 [N]

Gains	k	5 [N/m]
	ζ_0	0.1 [-]
	ζ_1	1.0 [-]
	Φ	1.5 [-]
	Γ	0.8 [-]
	c_1	0.0368 [Nms]
	c_2	0.0498 [Nms]
	c_3	0.0380 [Nms]
	c_4	0.0164 [Nms]

TABLE VIII

NUMERICAL VALUES OF INERTIA MATRIX $H(q(t))$ AT $t = 0$ IN THE CASE OF HAND-WRITING ROBOT (UNIT: kgm^2)

$$H(q(0)) = \begin{bmatrix} 2.955\times10^{-3} & 4.601\times10^{-6} & 4.601\times10^{-6} & 4.601\times10^{-6} \\ 4.601\times10^{-6} & 3.786\times10^{-3} & 1.579\times10^{-3} & 9.920\times10^{-5} \\ 4.601\times10^{-6} & 1.579\times10^{-3} & 1.300\times10^{-4} & 3.110\times10^{-4} \\ 4.601\times10^{-6} & 9.920\times10^{-5} & 3.110\times10^{-4} & 2.306\times10^{-4} \end{bmatrix}$$

Figures 11 and 12 show simulation results in the case that the initial values and gains are set as given in TABLE VII. In this case, numerical values of the inertia matrix at the initial time are shown in TABLE VIII. Then, by using eq.(21), joint damping factors c_i are determined in TABLE VIII. As seen in Fig.11, at the 10th trial it accurately follows the desired trajectory. Furthermore, although the feedforward torques to produce the desired pressing force are exerted at redundant joints, the pose of the robot does not become unnatural during its movement (e.g., the 3rd joint never contacts with the xy-plane). Figure 12 shows endpoint trajectories, and its time responses corresponding to x and y components and the pressing force λ at each trial. After a sufficient repetition of trials, the hand-writing robot can accomplish to write exactly the desired trajectory while generating the specified and commanded pressing force.

V. CONCLUSIONS

An iterative learning control scheme is proposed for robot arms with redundant joints relative to the number of physical variables describing a desired task. The learning update law is composed in task space by using descriptions of the desired task and measured data of physical variables only in task space. Convergence of trajectory trackings through repetition of trials is shown theoretically on the basis of an approximately linearized model. The effectiveness of the proposed method is verified by computer simulations on multi-joint reaching movements with redundant DOFs and hand-writings under a holonomic endpoint constraint.

Throughout the paper, existence of an ideal input $\boldsymbol{v}_d$ realizing the desired endpoint trajectory $\boldsymbol{x}_d(t)$ is assumed. This assumption can be validated by verifying that the system

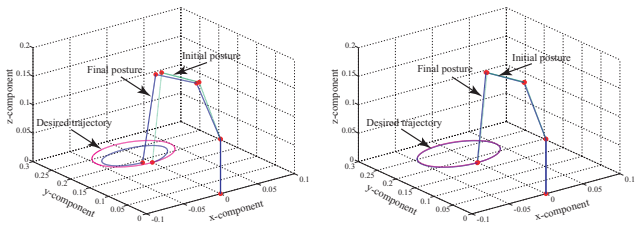

(a) 1st trial (b) 10th trial

Fig. 11. Endpoint trajectories and the initial and final postures of the robot

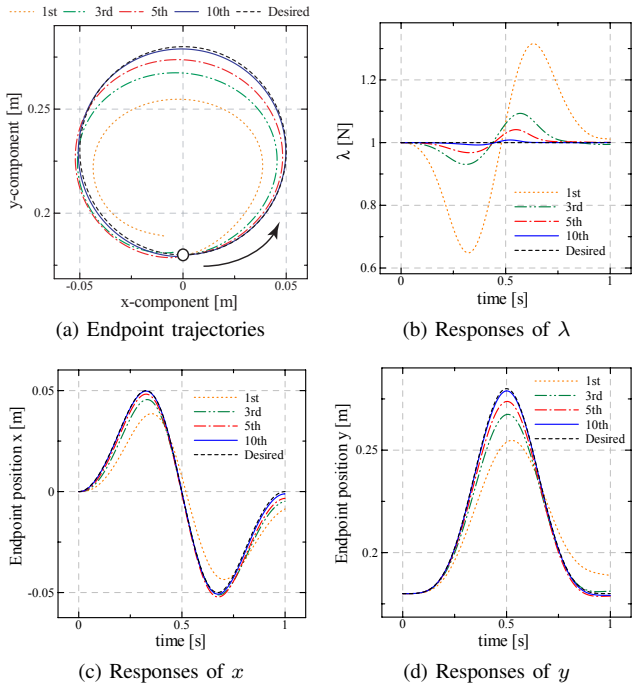

(a) Endpoint trajectories (b) Responses of λ

(c) Responses of x (d) Responses of y

Fig. 12. Transient responses in the case of movement by the hand-writing robot

of six simultaneous nonlinear differential equations

$$\dot{\boldsymbol{q}} = Q(\boldsymbol{q})\,(\dot{\boldsymbol{x}}_d^{\mathrm{T}},\ \dot{\boldsymbol{y}}_d^{\mathrm{T}})^{\mathrm{T}} \tag{30}$$

$$\ddot{\boldsymbol{y}}_d = -H_{22}^{-1}\left\{B_{22}\dot{\boldsymbol{y}}_d - H_{12}^{\mathrm{T}}\ddot{\boldsymbol{x}}_d - B_{21}\dot{\boldsymbol{x}}_d\right\} \tag{31}$$

concerning $(\boldsymbol{q}^{\mathrm{T}}, \dot{\boldsymbol{y}}_d^{\mathrm{T}})^{\mathrm{T}}$ has a unique solution. The rigorous proof of this claim will be presented elsewhere.

REFERENCES

[1] E. Thelen, D. Corbetta, K. Kamm, J. P. Spencer, K. Schneider, and R. F. Zernicke, "The transition to reaching : mapping intention and intrinsic dynamics : Developmental biodynamics : brain, body behavior connections," *Child Development*, vol. 64, no. 4, pp. 1058–1098, 1993.

[2] E. Thelen and L. Smith, *A Dynamic Systems Approach to the Development of Cognition and Action*. MA: MIT Press, 1994.

[3] S. Arimoto, S. Kawamura, and F. Miyazaki, "Bettering operation of robots by learning," *Journal of robotic systems*, vol. 1, no. 2, pp. 123–140, 1984.

[4] S. Arimoto, *Control Theory of Non-linear Mechanical Systems: A Passivity-based and Circuit-theoretic Approach*. Oxford, UK: Oxford Univ. Press, 1996.

[5] A. De Luca and F. Mataloni, "Learning control for redundant manipulators," in *Proc. of the 1991 IEEE International Conference on Robotics and Automation (ICRA1991)*, Sacramento, CA, Apr. 9-11 1991, pp. 1442–1450.

[6] S. Arimoto, M. Sekimoto, H. Hashiguchi, and R. Ozawa, "Natural resolution of ill-posedness of inverse kinematics for redundant robots: A challenge to Bernstein's degrees-of-freedom problem," *Advanced Robotics*, vol. 19, no. 4, pp. 401–434, 2005.
[7] S. Arimoto, H. Hashiguchi, M. Sekimoto, and R. Ozawa, "Generation of natural motions for redundant multi-joint systems: A differential-geometric approach based upon the principle of least actions," *Journal of Robotic Systems*, vol. 22, no. 11, pp. 583–605, 2005.
[8] S. Arimoto, H. Hashiguchi, and R. Ozawa, "A simple control method coping with a kinematically ill-posed inverse problem of redundant robots: Analysis in case of a handwriting robot," *Asian Journal of Control*, vol. 7, no. 2, pp. 112–123, 2005.
[9] J. Nakanishi, R. Cory, M. Mistry, J. Peters, and S. Schaal, "Comparative experiments on task space control with redundancy resolution," in *Proc. of the 2005 IEEE/RSJ Intl. Conf. on Intelligent Robots and Systems (IROS2005)*, Edmonton, Canada, Aug. 2-6 2005, pp. 1575–1582.
[10] A. De Luca, G. Paesano, and G. Ulivi, "A frequency-domain approach to learning control : implementation for a robot manipulator," *IEEE transactions on industrial electronics*, vol. 39, no. 1, pp. 1–10, 1992.
[11] H. Seraji, "Configuration control of redundant manipulators: theory and implementation," *IEEE Transactions on Robotics and Automation*, vol. 5, no. 4, pp. 472–490, 1989.
[12] H. Hashiguchi, S. Arimoto, and R. Ozawa, "Control of a handwriting robot with dof redundancy based on feedback in task coordinates," *Journal of Robotics and Mechatronics*, vol. 16, no. 4, pp. 381–387, 2004.

APPENDIX A

By subtracting $\boldsymbol{v}_d$ from the learning update law of eq.(3), we obtain

$$\Delta \boldsymbol{v}_{n+1} = \Delta \boldsymbol{v}_n - \Phi \Delta \dot{\boldsymbol{x}}_n \qquad (n = 0, 1, 2, \dots) \qquad \text{(A-1)}$$

Then, it follows that

$$\|\Delta \boldsymbol{v}_{n+1}(t)\|^2/2\Phi = \|\Delta \boldsymbol{v}_n(t)\|^2/2\Phi - \Delta \dot{\boldsymbol{x}}_n^{\mathrm{T}}(t)\Delta \boldsymbol{v}_n(t) + \Phi \|\Delta \dot{\boldsymbol{x}}_n(t)\|^2/2 \qquad \text{(A-2)}$$

Taking integral of this equation in t over $[0,\, t]$ yields

$$\begin{aligned}
&\int_0^t \left\{\|\Delta \boldsymbol{v}_{n+1}(\tau)\|^2/2\Phi\right\} \mathrm{d}\tau \\
&= \int_0^t \left\{\|\Delta \boldsymbol{v}_n(\tau)\|^2/2\Phi\right\} \mathrm{d}\tau - \{E_{dn}(t) - E_{dn}(0)\} \\
&\quad - \int_0^t \left\{ \left(\zeta_1 \sqrt{k} - \frac{\Phi}{2}\right) \|\Delta \dot{\boldsymbol{x}}_n(\tau)\|^2 \right. \\
&\qquad + (\Delta \dot{\boldsymbol{x}}_n^{\mathrm{T}}(\tau),\, \Delta \dot{\boldsymbol{y}}_n^{\mathrm{T}}(\tau))\; Q_d^{\mathrm{T}}(\tau) C Q_d(\tau) \\
&\qquad\qquad \left. (\Delta \dot{\boldsymbol{x}}_n^{\mathrm{T}}(\tau),\, \Delta \dot{\boldsymbol{y}}_n^{\mathrm{T}}(\tau))^{\mathrm{T}} \right\} \mathrm{d}\tau \\
&\le \int_0^t \left\{\|\Delta \boldsymbol{v}_n(\tau)\|^2/2\Phi\right\} \mathrm{d}\tau - E_{dn}(t) \\
&\qquad - \int_0^t \left(\zeta_1 \sqrt{k} - \frac{\Phi}{2}\right) \|\Delta \dot{\boldsymbol{x}}_n(\tau)\|^2 \mathrm{d}\tau \qquad \text{(A-3)}
\end{aligned}$$

since $E_{dn}(0) = 0$ and $Q_d^{\mathrm{T}}(\tau) C Q_d(\tau) \ge 0$. Therefore, if $0 < \Phi < 2\zeta_1 \sqrt{k}$ then for any $t \in (0,\, T]$

$$E_{dn}(t) \to 0 \quad \text{and} \quad \int_0^t \|\Delta \dot{\boldsymbol{x}}_n(\tau)\|^2 \mathrm{d}\tau \to 0 \qquad \text{(A-4)}$$

as $n \to \infty$. Referring to the form of E_{dn} defined in eq.(18), we can conclude that for any $t \in [0,\, T]$

$$\Delta \boldsymbol{x}_n(t) \to 0, \quad \Delta \dot{\boldsymbol{x}}_n(t) \to 0, \quad \Delta \dot{\boldsymbol{y}}_n(t) \to 0 \qquad \text{(A-5)}$$

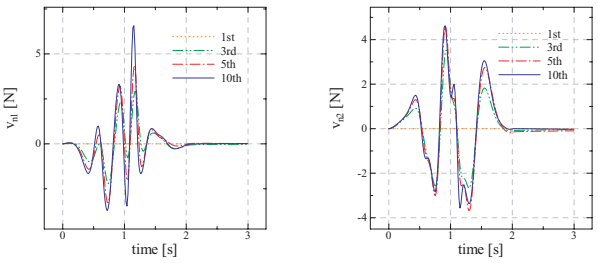

(a) v_{n1} (b) v_{n2}

Fig. 13. Transient responses of the ILC term $\boldsymbol{v}_n = (v_{n1}, v_{n2})^{\mathrm{T}}$

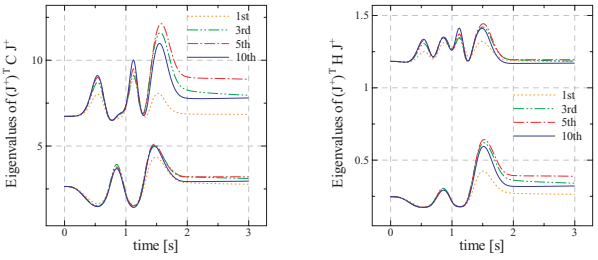

(a) $(J^+)^{\mathrm{T}} C J^+$ (b) $(J^+)^{\mathrm{T}} H J^+$

Fig. 14. Transient behaviours of eigenvalues

as $t \to \infty$. This completes the proof of convergence of trajectory trackings in task space under the assumption that the concerned dynamics can be expressed by the form of eq.(15). In this proof, we implicitly assumed the positive definiteness of matrix $(J_n^+)^{\mathrm{T}} C J_n^+$ during iteration of trials and also the convergence of $\boldsymbol{v}_n(t)$ to some idealized control signal (we denoted it by $\boldsymbol{v}_d(t)$). According to numerical simulations of trajectory tracking for the desired Lissajous figure, it is possible to show that both assumptions are valid as shown in Figs.13 and 14.

An extension of the proof to the case of hand-writing under a holonomic constraint is omitted in this paper due to page limitation.